Activated Switching in a Parametrically Driven Micromechanical Torsional Oscillator

H.B. Chan and C. Stambaugh

Parametric resonance and parametric amplification are important phenomena that are relevant to many fields of science. For mechanical systems, parametric driving typically involve modulating the spring constant [1, 2] or the moment of inertia near twice the natural frequency of the system. Parametric amplification has proved useful in improving the signal to noise before transduction of the mechanical displacement into an electrical signal [1]. Apart from amplifying a signal, parametric pumping can also reduce the linewidth of the resonance response, opening up new opportunities for biochemical detection using micro- and nano-mechanical devices in viscous environments [3]. Recently the sharp jump in the parametric response of micromechanical oscillators at subcritical bifurcation was used for accurate determination of the natural frequency to deduce device parameters [4].

Depending on the amplitude and frequency of the drive, a parametric oscillator possesses one, two or three stable states. Fluctuations induce transitions between coexisting attractors. The transition rate depends exponentially on the ratio of an activation barrier to the fluctuation intensity [5, 6]. Such dependence bears resemblance to equilibrium systems where the transition rate can be obtained from the height of the free energy barrier. However, the multistability in a parametric oscillator develops only when the system is under strong periodic drive. The system is far from thermal equilibrium and cannot be characterized by free energy [5]. Consequently, the transition rate needs to be calculated from system dynamics. Such fluctuation induced switching has been observed in a number of driven systems, including parametrically driven electrons in a Penning trap [7], micro- and nano-mechanical devices [8–11], radio frequency driven Josephson junctions [12–14] and atoms in magneto-optical traps [15, 16].

Here we describe our investigation of noise-activated switching in a parametrically driven micromechanical torsional oscillator. The electrostatic contribution to the spring constant is modulated near twice the natural frequency of the oscillator. When the parametric modulation is sufficiently strong, oscillations are induced at

H.B. Chan (✉)
Department of Physics, University of Florida, Gainesville, FL 32608, USA

V. In et al. (eds.), *Applications of Nonlinear Dynamics*, Understanding Complex Systems,
DOI 10.1007/978-3-540-85632-0_2,

half the modulation frequency. The phase of the oscillation can take on either one of two values that differ from each other by π. When noise is injected into the excitation voltage, the system can occasionally overcome the activation barrier and switch between the two states. The transition rates out of the two states are identical, yielding a dynamical bistable system that is driven out of equilibrium. As the parametric driving frequency approaches a bifurcation value, both the amplitude of oscillation and the activation barrier decrease and eventually become zero at the bifurcation frequency. Near the bifurcation frequency, we find that the activation barrier depends on frequency detuning with a critical exponent of 2, consistent with predicted universal scaling in parametrically driven systems [6]. Away from the vicinity of the bifurcation point, the dependence of the activation barrier on frequency detuning crosses over from quadratic to 3/2th power dependence that is specific to our device.

In our experiment, the micromechanical oscillator is fabricated using a surface micromachining process on a silicon substrate. As shown in Fig. 1a, the oscillator consists of a polysilicon plate (500 µm by 500 µm by 3.5 µm) supported by two torsional rods. By etching away a 2-µm-thick sacrificial silicon oxide layer beneath the top plate, the top plate becomes free to rotate about the torsional rods. The other ends of the torsional rods are anchored to the substrate (Fig. 1b). Two fixed polysilicon electrodes are located below the top plate. One of the electrodes is used to modulate the spring constant electrostatically and the other electrode is used to capacitively detect motions of the top plate.

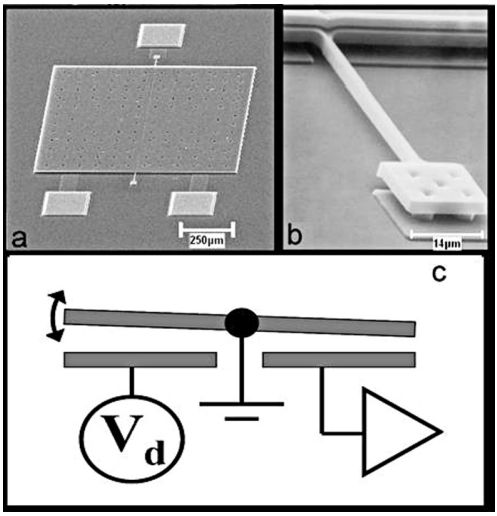

Fig. 1 (**a**) Scanning electron micrograph of the torsional oscillator. The large square in the middle is a movable polysilicon plate. The small squares are wire-bond pads that provide electrical connections to the top plate and the two fixed electrodes. (**b**) Close up on one of the torsional springs. (**c**) Cross sectional schematic of the oscillator with measurement circuitry

Figure 1c shows a cross-sectional schematic of the oscillator with electrical connections. The application of a periodic voltage with dc bias to the left electrode exerts an electrostatic torque on the grounded top plate. Modulations of the restoring torque are generated by the periodic component of the applied voltage. As the plate oscillates, the capacitance between the plate and the detection electrode changes. The detection electrode is connected to a charge sensitive preamplifier followed by a lock-in amplifier that measures the signal at the half the modulation frequency. Measurements were performed at liquid nitrogen temperature and at pressure of less than 1×10^{-6} *torr*. The quality factor Q of the oscillator exceeds 7,500.

The modulations of the spring constant in our torsional oscillator originate mainly from the strongly distance-dependent electrostatic interaction between the top plate and the excitation electrode. The equation of motion of the oscillator is given by:

$$\ddot{\theta} + 2\gamma\dot{\theta} + \omega_0^2\theta = \tau/I \tag{1}$$

where θ is the angular rotation of the top plate, γ is the damping coefficient and ω_0 is the natural frequency of the oscillator. The driving torque τ arises from the electrostatic interaction between the top plate and the driving electrode:

$$\tau = \frac{1}{2}\frac{dC}{d\theta}V_d^2 \tag{2}$$

where C is the capacitance between the top plate and the driving electrode. A Taylor expansion of τ about the equilibrium angular position θ_0 yields:

$$\tau = \frac{1}{2}\left(C'(\theta_o) + C''(\theta_o)\theta + \frac{1}{2}C'''(\theta_o)\theta^2 + \frac{1}{6}C''''(\theta_o)\theta^3\right)V_d^2 \tag{3}$$

where C', C'', C''' and C'''' denote the first, second, third and fourth angular derivative of C respectively. The excitation voltage V_d is a sum of three components:

$$V_d = V_{dc} + V_{ac}\sin(\omega t) + V_{noise}(t) \tag{4}$$

The three terms on the right side of Eq. (4) represent the dc voltage, periodic ac voltage and random noise voltage respectively. V_{dc} is chosen to be much larger than V_{ac} and V_{noise} to partially linearize the dependence of τ on V_{ac} and V_{noise}. The strong angular dependence of the electrostatic torque leads to nonlinear contributions to the restoring torque. Substituting V_d and τin Eqs. (1) and (2) leads to:

$$\ddot{\theta} + 2\gamma\dot{\theta} + \left[\omega_0^2 + \frac{k_o}{I} + \frac{K_e}{I}\cos(\omega t)\right]\theta + \alpha\theta^2 + \beta\theta^3 + D = N(t) + F\cos(\omega t) \tag{5}$$

where $\alpha = -C'''(\theta_o)V_{dc}^2/4I$, $\beta = -c''''(\theta_o)V_{dc}^2/12I$, $D = -C'(\theta_o)V_{dc}^2/2I$, $F = C'(\theta_o)V_{dc}V_{ac}(t)/I$, $k_o = -C''(\theta_o)V_{dc}^2/2$, $N(t) = -C'(\theta_o)V_{dc}V_{noise}(t)/I$ is the effective noise in the excitation and $k_e + -C''(\theta_o)V_{dc}V_{ac}$ is the effective amplitude of the modulation of spring constant. Coupling of the electrostatic torque

$F\cos(\omega t)$ and the nonlinear terms generates an effective modulation of spring constant. However, this contribution is much smaller than the direct electrostatic modulation of the spring (k_e/I). As a result, the $F\cos(\omega t)$ term can be neglected. After redefining the angle to be measured from the equilibrium angular position θ_0, the equation of motion reduces to [17]:

$$\ddot{\theta} + 2\gamma\dot{\theta} + \left[\omega_1^2 + \frac{k_e}{I}\cos(\omega t)\right]\theta + \alpha\theta^2 + \beta\theta^3 = N(t) \tag{6}$$

where $\omega_1^2 = \omega_o^2 + k_o/I$.

We first focus on the response of the oscillator with no injected noise in the excitation. When the electrostatic spring modulation is small, there are no induced oscillations at $\omega/2$. It is necessary for the amplitude of spring modulation to reach a threshold value of $k_T = 4\omega_o\gamma I$ before oscillations are induced at half the modulation frequency in a range close to ω_o. As shown in Fig. 2, there are three ranges of frequencies with different numbers of stable attractors, separated by a supercritical bifurcation point $\omega_{b1} = 2\omega_o + \omega_p$ and a subcritical bifurcation point $\omega_{b1} = 2\omega_o - \omega_p$, where $\omega_p = \sqrt{k_e^2 - k_T^2}/2I\omega_o$. In the first region ($\omega > \omega_{b1} \sim 41174$ rad s^{-1}), no oscillations take place, as the only stable attractor is a zero-amplitude state. At ω_{b1}, there emerge two stable states of oscillations at frequency $\omega/2$ that differ in phase by π but are otherwise identical. This symmetry is illustrated in Fig. 3a, where the period of the induced oscillation is twice that of the parametric driving. In Fig. 3b, both the drive and response are shifted in time by $2\pi/\omega$. While the drive remains unchanged, the response has picked up an extra phase of π. Both oscillation states are valid solutions of Eq. (6). Their amplitudes are the same but their phase differs by π. These two stable states are separated in phase space by an unstable state with zero oscillation amplitude (dotted line in Fig. 2). At frequencies below $\omega_{b2}(\sim 41150$ rad s$^{-1})$, the zero-amplitude state becomes stable, resulting in the coexistence

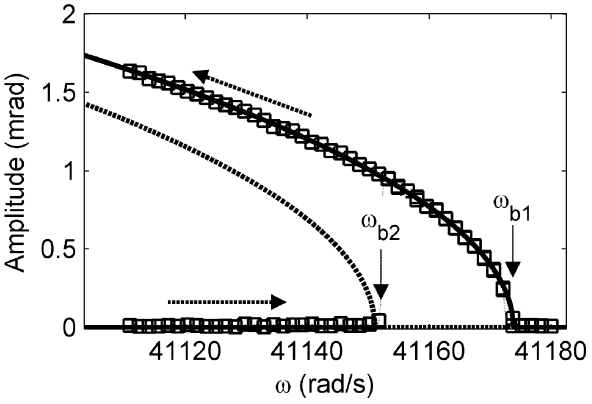

Fig. 2 Oscillation amplitude at $\omega/2$ vs frequency of parametric modulation ω. The solid and dotted lines represent the stable and unstable oscillation states respectively

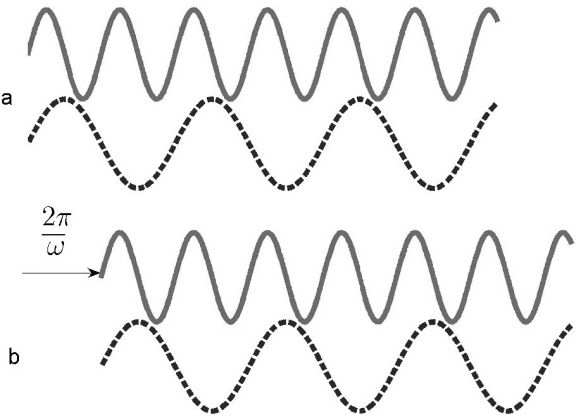

Fig. 3 Two coexisting oscillation states of the parametric oscillator. The red lines represent the parametric modulation. The two blue lines in (**a**) and (**b**) shows the two stable states with the same oscillation frequency but opposite phase

of three stable attractors. These stable states are separated in phase space by two unstable states indicated by the dotted line in Fig. 2.

In the presence of noise in the excitation, the oscillator could be induced to switch between coexisting attractors. Since the parametric oscillator is a driven system that is far from thermal equilibrium and cannot be characterized by free energy, calculation of the escape rate is a non-trivial problem. Theoretical analysis suggests that the rate of escape Γ at a particular driving frequency depends exponentially on the ratio of an activation barrier R to the noise intensity I_N [5]:

$$\Gamma = \Gamma_0 \exp(-R/\mathrm{I}_N) \tag{7}$$

In general, R depends on various device parameters including the natural frequency, the parametric driving frequency, the damping constant and the nonlinear coefficients. Near the bifurcation points, the system dynamics is characterized by an overdamped soft mode and R decreases to zero according to $k|\omega - \omega_b|^{\xi}$ with a critical exponent ξ that is system independent [5]. While the prefactor k might be different for each system, ξ is universal for all systems and depends only on the type of bifurcation. For instance, a Duffing oscillator resonantly driven into bistability undergoes spinodal bifurcations at the boundaries of the bistable region. One stable state merges with the unstable state while the other stable state remains far away in phase space. Recent experiments in micromechanical oscillators [9] and rf-driven Josephson junctions [18] have confirmed the theoretical prediction [5, 19] that the activation barrier scales with critical exponent 3/2 near spinodal bifurcations in driven systems. On the other hand, in a parametric oscillator, the supercritical and subcritical bifurcations involve the merging of two stable oscillation states and an unstable zero-amplitude state (at ω_{b1}) and the merging of two unstable states and a zero-amplitude stable state (at ω_{b2}) respectively. When three states merge together in such pitchfork bifurcations, the critical exponent is predicted to be 2. Away from

the bifurcation points, the scaling relationship no longer holds and different exponents were obtained depending on the nonlinearity and damping of the system.

In our experiment, we inject $V_{noise}(t)$ with a bandwidth of $\sim$300 rad s^{-1}centered at ω_o to induce the transitions between stable states in our parametric oscillator. The bandwidth of the noise is much larger than the resonance linewidth. Figure 4a and 4c show respectively the oscillation amplitude and phase at a driving frequency between ω_{b2} and ω_{b1}, in the range of two coexisting attractors. The oscillator resides in the one of the oscillation state for various durations before escaping to the other state. Transitions take place when the phase slips by π. The two oscillation states have the same amplitude. These two attractors can also be clearly identified in the occupation histograms in Fig. 5a and 5b. Figure 4b and 4d show switching events at a driving frequency lower than ω_{b2}, with three attractors. The zero-amplitude state has also become stable. Unlike Fig. 4a, the oscillator switches between two distinct amplitudes. At high amplitude, the phase takes on either one of two values that differ by π. When the oscillator is in the zero-amplitude state, there are large fluctuations of the phase as a function of time as the oscillator moves about the origin. The coexistence of three attractors in phase space is also illustrated in Fig. 5c and 5d for two other driving frequencies.

Figure 6a shows a histogram of the residence time in one of the oscillation states before a transition occurs. The exponential dependence on the residence time indicates that the transitions are random and follow Poisson statistics as expected. An exponential fit to the histogram yields the transition rate. The transition rates out of the two oscillation states are measured to be identical to within experimental

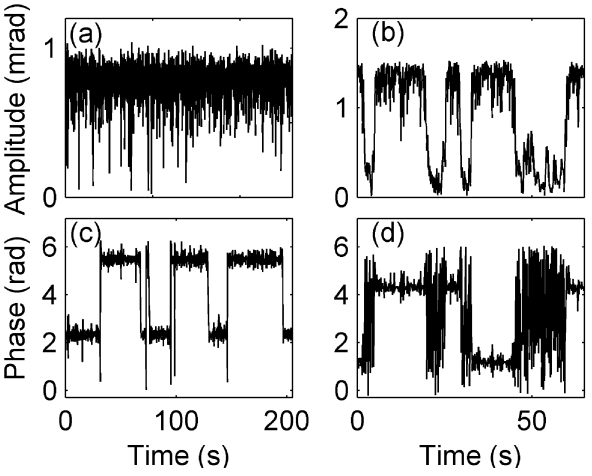

Fig. 4 Oscillation amplitude (**a**) and phase (**c**) for a driving frequency of 41159.366 rad s^{-1}. In the range $\omega_{b2} < \omega < \omega_{b1}$ transitions take place when the phase slips by π (**b**) When ω (41124.705 rad s^{-1}) is lower than ω_{b2} , transitions occur with jumps in the amplitude. (**d**) The phase differs by π for the two high amplitude states. When the oscillator is in the zero-amplitude state, there are large fluctuations in the phase

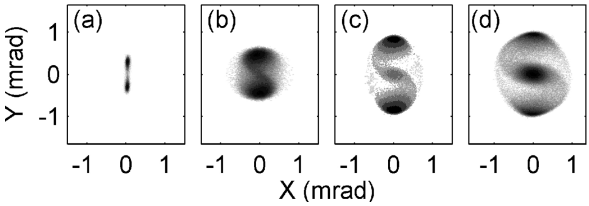

Fig. 5 Phase space occupation for four different modulation frequencies. X and Y represent the amplitudes of the two quadratures of oscillation that are out of phase with each other. Darker grey scale corresponds to higher occupation. (**a**) $\omega = 41171.6$ rad s^{-1}. Two oscillation states coexist near ω_{b1}. (**b**) $\omega = 41163.0$ rad s^{-1}. The two states move further apart as ω decreases. (**c**) $\omega = 41139.8$ rad s^{-1}. The zero-amplitude states becomes stable. (**d**) $\omega = 41124.8$ rad s^{-1}. The occupation of the zero-amplitude state increases as ω decreases

uncertainty at all noise intensities. Figure 6b plots the logarithm of the transition rate as a function of inverse noise intensity. The transition rate depends exponentially on inverse noise intensity, demonstrating that switching between the states is activated in nature. According to Eq. (7), the slope in Fig. 6b yields the activation barrier at the particular detuning frequency. Transitions were also measured for switching out of the zero-amplitude state for $\omega < \omega_{b2}$. These switches were also found to be activated and follow Poisson statistics in a similar manner.

We repeat the above procedure to determine the activation barriers at other driving frequencies. Figure 7a plots the activation barriers R_1 for switching out of the oscillation states and R_2 for switching out of the zero-amplitude state as a function of the driving frequency. When the driving frequency is high, only the zero-amplitude state is stable. With decreasing frequency, two stable oscillation states (separated by an unstable state) emerge at ω_{b1}. As the detuning $\Delta\omega_1 = \omega_{b1} - \omega$ increases, the pair of oscillation states move further apart in phase space and R_1 increases. At ω_{b2}, the zero-amplitude state becomes stable. The appearance of the stable zero-amplitude state is accompanied by the creation of two unstable states separating it in phase space from the two stable oscillation states. Initially, R_2 increases with frequency detuning $\Delta\omega_2 = \omega_{b2} - \omega$ in a fashion similar to R_1. Close to ω_{b2}, R_1 is larger than

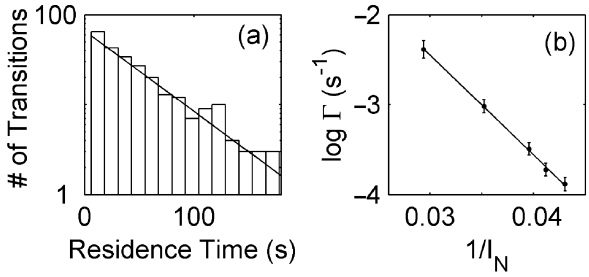

Fig. 6 (**a**) Histogram of the residence time in one of the oscillation states at ω = 41130.49 rad s^{-1} on semi-logarithmic scale, fitted by an exponential decay (solid line). (**b**) Dependence of the logarithm of the transition rate on the inverse noise intensity

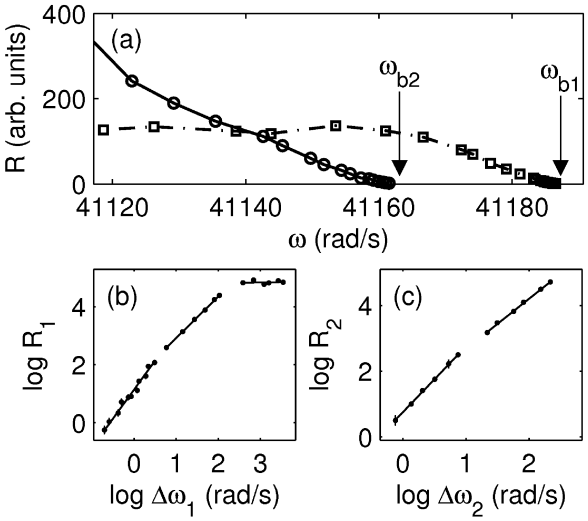

Fig. 7 (**a**) The activation barriers R_1 and R_2 vs. the parametric modulation frequency. (**b**) log R_1 vs. log $\Delta\omega_1$. (**c**) log R_2 vs. log $\Delta\omega_2$. The lines are power law fits to different ranges of $\Delta\omega$

R_2 and the occupation of the oscillation states is higher than the zero-amplitude state. As the frequency decreases, R_2 continues to increase monotonically while R_1 remains approximately constant. As a result, R_1 and R_2 cross each other at ~ 41140 rad s^{-1}, beyond which the occupation of the zero-amplitude state becomes higher than the oscillation states. The dependence of the occupation on frequency detuning was also observed in parametrically driven atoms in magneto-optical traps [15].

Figure 7b and 7c show the dependence of the activation barriers $R_{1,2}$on $\Delta\omega_{1,2}$ on logarithmic scales. When the detuning is small, both R_1 and R_2 show power law dependence on $\Delta\omega$. From the linear fits, the exponents are measured to be 2.0 ± 0.1 and 2.00 ± 0.03 for R_1 and R_2 respectively. Such quadratic dependence of the activation barrier on detuning near the bifurcation points is predicted to be system-independent [5,6] and is expected to occur in other parametrically-driven, nonequilibrium systems such as electrons in Penning traps [7] and atoms in magneto-optical traps [15,16]. Away from the vicinity of the bifurcation point, however, the variation of the activation barrier with frequency detuning becomes device-specific. Figure 7b and 7c show crossovers from the quadratic dependence to different power law dependence with exponents 1.43 ± 0.02 and 1.53 ± 0.02 for R_1 and R_2 respectively. These values obtained in our experiment are distinct from the exponents obtained in parametrically driven electrons in Penning traps [7] because the nonlinearity and damping are different for the two systems.

Recent theoretical predictions indicate that the symmetry in the occupation of the two oscillation states in a parametrically driven oscillator will be lifted when an additional small drive close to frequency $\omega/2$ is applied [20]. A number of phenomena, including strong dependence of the state populations on the amplitude of

the small drive and fluctuation enhanced frequency mixing, are expected to occur. Experiments are underway to test such predictions and to reveal other fluctuation phenomena in parametrically driven oscillators.

We are grateful to M. I. Dykman and D. Ryvkine for useful discussions. This work was supported by NSF DMR-0645448.

References

1. D. Rugar and P. Grutter, Phys. Rev. Lett. **67**, 699 (1991).
2. D. W. Carr, S. Evoy, L. Sekaric, et al., Appl. Phys. Lett. **77**, 1545 (2000).
3. L. Sekaric, M. Zalalutdinov, R. B. Bhiladvala, et al., Appl. Phys. Lett. **81**, 2641 (2002).
4. W. H. Zhang, R. Baskaran, and K. L. Turner, Sensors and Actuators a-Physical **102**, 139 (2002).
5. M. I. Dykman and M. A. Krivoglaz, Zh. Eksper. Teor. Fiz. **77**, 60 (1979).
6. M. I. Dykman, C. M. Maloney, V. N. Smelyanskiy, et al., Phys. Rev. E **57**, 5202 (1998).
7. L. J. Lapidus, D. Enzer, and G. Gabrielse, Phys. Rev. Lett. **83**, 899 (1999).
8. J. S. Aldridge and A. N. Cleland, Phys. Rev. Lett. **94**, 156403 (2005).
9. C. Stambaugh and H. B. Chan, Phys. Rev. B **73**, 172302 (2006).
10. R. L. Badzey and P. Mohanty, Nature **437**, 995 (2005).
11. R. Almog, S. Zaitsev, O. Shtempluck, et al., Appl. Phys. Lett. **90**, 013508 (2007).
12. E. V. Sukhorukov and A. N. Jordan, Phys. Rev. Lett. **98**, 136803 (2007).
13. I. Siddiqi, R. Vijay, F. Pierre, et al., Phys. Rev. Lett. **93**, 207002 (2004).
14. I. Siddiqi, R. Vijay, F. Pierre, C. M. Wilson, L. Frunzio, M. Metcalfe, C. Rigetti, R. J. Schoelkopf, M. H. Devoret, D. Vion, and D.Esteve, Phys. Rev. Lett. **94**, 027005 (2005).
15. K. Kim, M. S. Heo, K. H. Lee, et al., Phys. Rev. A **72**, 053402 (2005).
16. K. Kim, M. S. Heo, K. H. Lee, et al., Phys. Rev. Lett. **96**, 150601 (2006).
17. L. D. Landau and E. M. Lifshitz, *Mechanics, Course of theoretical physics vol.1*, (1969).
18. I. Siddiqi, R. Vijay, F. Pierre, et al., cond-mat/0507248 (2005).
19. M. I. Dykman, I. B. Schwartz, and M. Shapiro, Phys. Rev. E **72**, 021102 (2005).
20. D. Ryvkine and M. I. Dykman, Phys. Rev. E **74**, 061118 (2006).

http://www.springer.com/978-3-540-85631-3

Applications of Nonlinear Dynamics
Model and Design of Complex Systems
In, V.; Longhini, P.; Palacios, A. (Eds.)
2009, XIV, 478 p., Hardcover
ISBN: 978-3-540-85631-3